ACT Project Number:
271498

Project name:
ELEGANCY

Project full title:
Enabling a Low-Carbon Economy via Hydrogen and CCS

ERA-Net ACT project

Starting date: 2017-08-31
Duration: 36 months

D2.1.5
Solubility of H₂ in Pure Water at Reservoir Conditions

Date: 2019-03-31

Organization name of lead participant for this deliverable:
Imperial College London

Deliverable number:	D2.1.5
Deliverable title:	Solubility of H_2 in Pure Water at Reservoir Conditions
Work package:	WP 2 CO_2 transport, injection and storage
Lead participant:	ICL

Authors		
Name	Organization	E-mail
Geraldine Torín-Ollarves	ICL	g.torin-ollarves@imperial.ac.uk
J P Martin Trusler*	ICL	m.trusler@imperial.ac.uk

*Mark Lead Author with asterix

Keywords
Brine; Hydrogen; Solubility; Water

Abstract
The apparatus detailed in deliverable D2.1.4 has been employed to make measurements of the solubility of hydrogen in pure water. The experimental protocol has been further refined from that reported in D2.1.4 and the rates of interfacial mass transfer have been estimated. Additional solubility data have been retrieved from the literature and the combined results fitted to a correlative thermodynamic model. The report details the new experimental protocol and results obtained from the experiment and modelling. The correlative model reported is valid at temperatures between 273.15 K and 373.15 K and at pressures up to 101 MPa.

TABLE OF CONTENTS

1 INTRODUCTION

Reliable knowledge of the thermophysical properties of mixtures of CO_2 and numerous other substances are essential in designing the overall process of hydrogen production from fossil fuels with simultaneous capture, transportation and storage of CO_2. Captures CO_2 is never pure, and, in this process, hydrogen is likely to be a significant impurity. This will affect the properties of the CO_2-rich stream during pipeline transportation and influence the storage behavior once the fluid is injected into a storage reservoir [1]. In the case of aquifer storage, the key components of interest are CO_2, impurities including H_2, water, salts and the reservoir minerals with which these fluids are in contact. In the ELEGANCY project, one of the objectives is to improve the available thermodynamic-property models to encompass hydrogen and other impurities both under the conditions of pipeline transportation and under aquifer-storage reservoir conditions.

The specific objectives of Task 2.1 "Thermodynamic property model for CO_2-brine" are to:
- Study the solubility behavior of $CO_2 + H_2$ in water and brines at reservoir conditions
- Develop a thermodynamic-property model to represent both this solubility behavior and the thermodynamic properties of the coexisting phases.

This report addresses the measurement of H_2 solubility in pure water, including a detailed mathematical model of the measurement system, and the correlation of the available solubility data in terms of a thermodynamic model.

2 PROTOCOL FOR SOLUBILITY MEASUREMENTS

2.1 Resume of experimental system and procedure

The experimental apparatus developed in this project is detailed in D2.1.4. Figure 2.1 is the PFD of the measurement system built up around a bespoke high-pressure view cell.

Figure 2.1: PFD of the system. SP, syringe pump; P_G & P, pressure sensors; T, temperature sensor; HJ, heating jacket; C, camera; RD, rupture disk; V1, V2, pump fill and dispense valve; V3, V4, V6, V8, manual valves; V5 & V7, proportional relief valves.

The standard operating procedure (SOP) for the experiment on H_2 solubility, starting with a clean and evacuated system, was as follows (with reference to Fig 2.1):

1. Fill the liquid bottle with pure water.
2. Set the desired operating temperature.
3. Close V2, open V1 and allow water to flow into the evacuated pump.
4. Close V1, raise pressure in the pump and purge to waste through V2 and V3. Refill the pump though V1.
5. Isolate the outlet of the cell at V6 and isolate the liquid inlet at V3.
6. Slowly open V4 and admit gas until a pre-determined filling pressure is reached.
7. Allow the system to reach equilibrium and record the cell temperature and the pressure of the gas (measured with P_G).
8. Turn on the stirring mechanism, open valve V2 and V3, and start to transfer liquid into the cell.
9. When the cell is nearly filled with liquid, stop the transfer of liquid and continue stirring until the system reaches equilibrium in the two-phase region. At this point there should be a small bubble of gas remaining.
10. Proceed with further small injections of liquid (e.g. 0.2 mL) and equilibration periods until the bubble is completely dissolved.

11. Make a few further injections to raise the pressure in the single-phase region.
12. At the conclusion of the measurement, discharge the cell contents to waste through V6. The cell temperature may also be elevated above the boiling point of water to help empty the cell.
13. Finally, evacuate the system, through V6 and V8.
14. If, during steps 12 and 13, the syringe pump is not emptied then, in a subsequent experiment, steps 3 and 4 are unnecessary.

This SOP is slightly different to the one described in D2.1.4 for CO_2 dissolution; the modified SOP was found to be more suitable for sparingly-soluble gases such as H_2.

To determine the bubble point, the equilibrium pressures recorded in steps 9 to 11 can be plotted against the volume of water injected as illustrated in Figure 2.2. The intersection of regression lines in the two-phase and single-phase regions identifies the bubble pressure. The amount of gas present is determined from the initial filling pressure and temperature and the amount of water present at the bubble point is determined from the volume V_{in} injected and the temperature and pressure in the syringe pump. Hence the bubble pressure and composition are both determined. Here, the single-phase region is fitted with a linear function of V_{in} while the two-phase data are fitted to a quadratic.
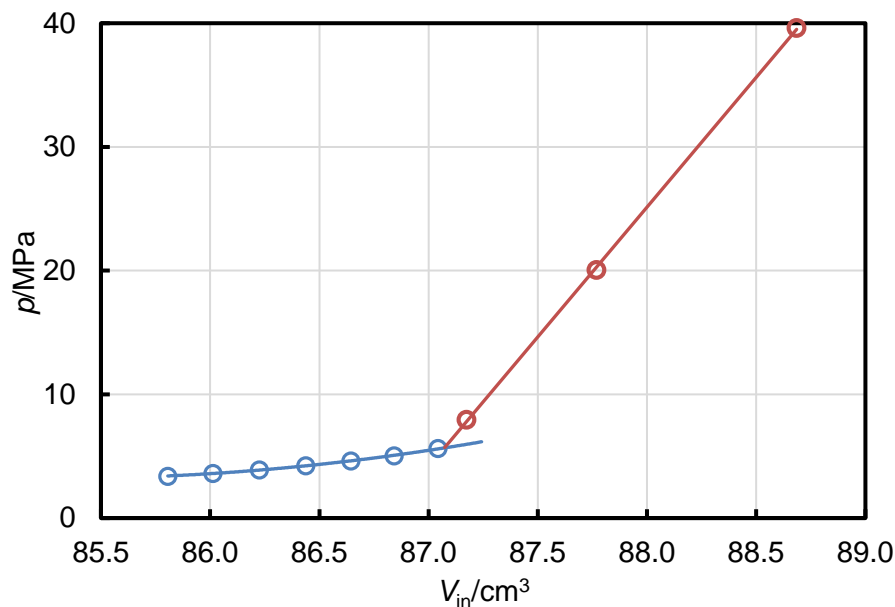

Figure 2.2: Pressures in the two-phase and single-phase regions for H_2 solubility in water. Symbols: O, experiment (two phases); O, experiment (one phase). Solid lines: regression functions.

An alternative plot which can be used for the same purpose is shown in figure 2.3. The advantage of this plot is the pressure in the two-phase region are nearly linear in V_{in}, while those in the single-phase region are the inverse of a linear function. This makes the fitting of the data more reliable.
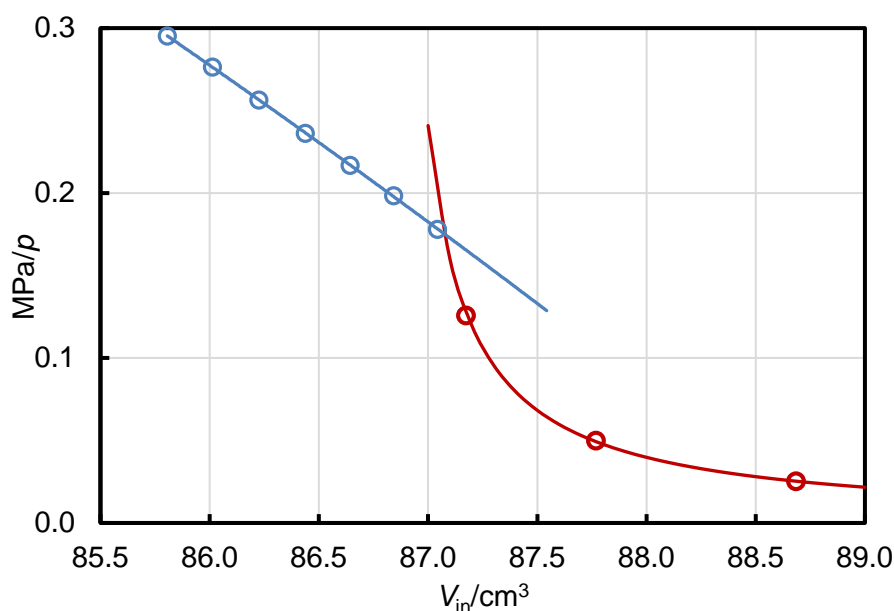
Figure 2.3: Inverse of the pressures in the two-phase and single-phase regions for H₂ solubility in water. Symbols: ○, experiment (two phases); ○, experiment (one phase). Solid lines: regression functions.

A less-empirical procedure can also be used in which a detailed thermodynamic model is fitted to the experimental data as discussed further below in section 2.3.

2.2   Rate of interfacial mass transfer and required equilibrations time

Following each injection of water, the cell pressure was monitored as a function of time as the system approached equilibrium. Given the very small amounts of water injected at high pressures, the controlling factor in this equilibration process was the rate of interfacial mass transfer rather than other factors such as thermal equilibration. The time constant for the approach to equilibrium was determined by fitting exponential decay curves to the pressure-time data as illustrated in Figure 2.4. These accounted very well for the observed behavior. It was noted that the time constant τ in this model depended somewhat on the stirring rate but experiments were generally carried out at the fastest possible stirring rate and the time constant then depended mainly on the size of the remaining bubble. As this decreased, the surface area available for mass transfer decreased and the time required for equilibration increased. An approximately-linear correlation was observed between $1/\tau$ and the volume of the remaining gas bubble with the time constant ranging from just a few minutes, far from the bubble point, to about 25 min close to the bubble point. Knowledge of this behavior is extremely useful in the design of the experimental protocol.
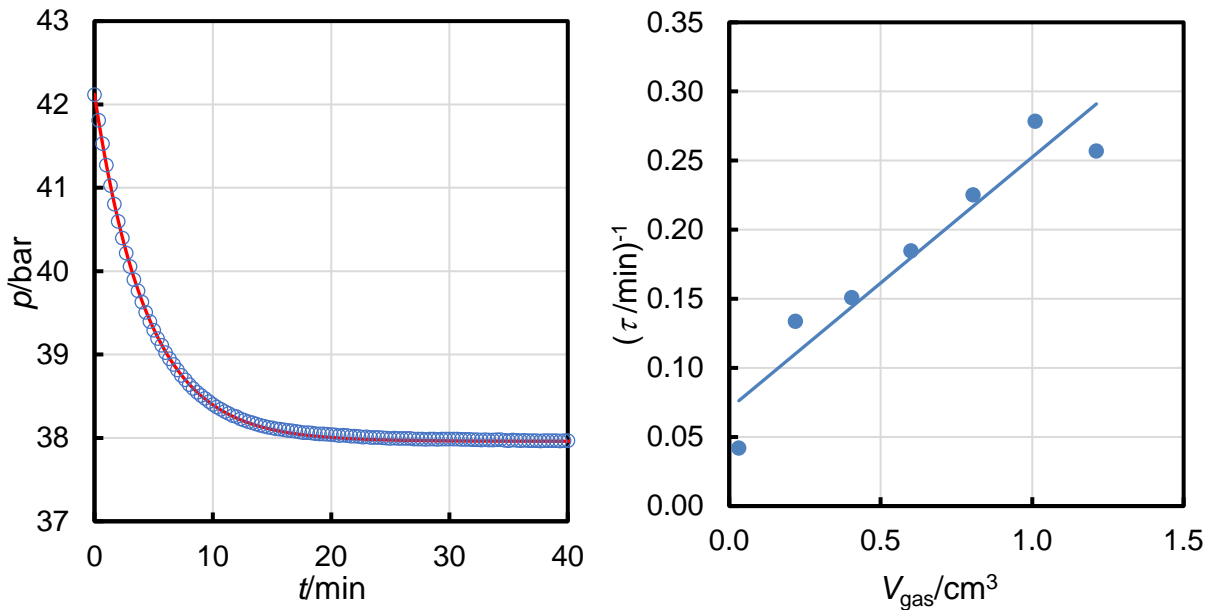
Figure 2.4: Left: Approach to equilibrium during H_2 dissolution into H_2O at $T = 323.15$ K. Right: Correlation between the inverse of the equilibration time constant τ and the volume V_{gas} of undissolved gas remaining in the solubility cell. Symbols: experimental data. Solid red curve, exponential decay curve. Solid blue line, linear regression.

2.3   Thermodynamic model of the solubility experiment

The experiment to be modelled is one in which a cell, maintained at constant temperature and initially filled with a charge of gas, is subject to step-wise injection of liquid solvent from a calibrated pump. After each injection, the system is stirred until equilibrium is achieved and the pressure is measured. A plot of the equilibrium pressure against the amount of solvent injected is characterized by a two-phase region in which the pressure rises slowly with each injection, switching to a rapidly-rising single-phase region above the bubble point, as illustrated above in figure 2.2. The intersection of these two branches permits determination of the composition and the pressure at the bubble point.

In the following, let 1 denote the solvent and 2 denote the solute gas. The notation to be used in the analysis is detailed in Table 2.1.

In the two phase-region, the necessary conditions for thermodynamic equilibrium between the coexisting phases are: (1) equality of temperatures; (2) equality of pressures; and (3) equality of the liquid-phase and vapor-phase fugacities of each component. Using the so-called asymmetric approach, the fugacities of the components in the gas and liquid phases are given by

$$
\left.
\begin{aligned}
f_{1,\mathrm{g}} &= y_1 \varphi_1 p \\
f_{1,\mathrm{L}} &= x_1 \varphi_{1,\mathrm{sat}} p_{1,\mathrm{sat}} \gamma_1 \exp\left(\int_{P_{1,\mathrm{sat}}}^{p} (v_1 / RT)\, dp \right) \\
f_{2,\mathrm{g}} &= y_2 \varphi_2 p \\
f_{2,\mathrm{L}} &= x_2 k_{\mathrm{H}} \gamma_2 \exp\left(\int_{P_{1,\mathrm{sat}}}^{p} (v_2 / RT)\, dp \right)
\end{aligned}
\right\}.
\tag{1}
$$

Table 2.1: Definition of symbol used in the thermodynamic model.

Symbols	Definition
β	Vapor fraction
x_i, y_i	Mole fractions of component i in the liquid, vapor phase
z_i	Overall mole fraction of component i in the system
K_i	Vaporization equilibrium ratios $= y_i/x_i$
$p_{1,\mathrm{sat}}$	Vapor pressure of the solvent at the system temperature
$\varphi_{1,\mathrm{sat}}$	Fugacity coefficient of the saturated solvent
$f_{i,\mathrm{L}}, f_{i,\mathrm{g}}$	Fugacities of component i in the liquid, vapor phase
$\varphi_{i,\mathrm{L}}, \varphi_{i,\mathrm{g}}$	Fugacity coefficients of component i in the liquid, vapor phase
γ_i	Activity coefficient of component i in the liquid phase
B_{ij}	Interaction second virial coefficient for i-j pair
C_{ijk}	Interaction third virial coefficient for i-j-k triplet
k_{H}	Henry's constant for gaseous solute
n_i	Amount of substance i in the system
n	Total amount of all substances present in the system
v_1	Partial molar volume of the solvent
v_2	Partial molar volume of the gaseous solute at infinite dilution
v_{L}	Molar volume of the mixed liquid phase
v_{G}	Molar volume of the gas phase
V_{L}	Volume filled by the liquid phase
V_{cell}	System (cell) volume
V_{o}	System (cell) volume at zero pressure
χ	Pressure coefficient of the system volume
Z	Compression (or compressibility) factor of the gas phase

In a dilute solution (sparingly-solute gas), the activity coefficients γ_i can be set equal to unity, v_1 can be set equal to the molar volume of the pure solvent and v_2 can be identified as the partial molar volume of the solute at infinite dilution. The vaporization equilibrium ratios are then given by

$$
\left.
\begin{aligned}
K_1 &= \frac{y_1}{x_1} = \left(\frac{\varphi_{1,\mathrm{sat}} p_{1,\mathrm{sat}}}{\varphi_1 p} \right) \exp\left(\int_{P_{1,\mathrm{sat}}}^{p} (v_1 / RT)\, dp \right) \\
K_2 &= \frac{y_2}{x_2} = \left(\frac{k_{\mathrm{H}}}{\varphi_2 p} \right) \exp\left(\int_{P_{1,\mathrm{sat}}}^{p} (v_2 / RT)\, dp \right)
\end{aligned}
\right\}.
\tag{2}
$$

At moderate pressures, the virial equation of state truncated after the third virial coefficient may be used for the vapor phase:

$$Z = 1 + B / v_G + C / v_G^2. \tag{3}$$

Here, $Z = p v_G / RT$ is the compression factor, v_G is the molar volume of the gas, and B and C are the second and third virial coefficients of the mixture. Written for a binary mixture, the second virial coefficient is given by

$$B = y_1^2 B_{11} + 2 y_1 y_2 B_{12} + y_2^2 B_{22}, \tag{4}$$

where B_{ii} is the second virial coefficient of pure component i and B_{12} is the interaction virial coefficient. The third virial coefficient is given for the binary mixture by

$$C = y_1^3 C_{111} + 3 y_1^2 y_2 C_{112} + 3 y_1 y_2^2 C_{122} + y_2^3 C_{222}, \tag{5}$$

where C_{iii} is the third virial coefficient of pure component i and C_{112} and C_{122} are the two possible interaction third virial coefficient. In terms of this equation of state, the fugacity coefficients are given by

$$\left. \begin{aligned} \ln \varphi_1 &= 2(y_1 B_{11} + y_2 B_{12})v_G^{-1} + (3/2)(y_1^2 C_{111} + 2 y_1 y_2 C_{112} + y_2^2 C_{122})v_G^{-2} - \ln Z \\ \ln \varphi_2 &= 2(y_1 B_{12} + y_2 B_{22})v_G^{-1} + (3/2)(y_1^2 C_{112} + 2 y_1 y_2 C_{122} + y_2^2 C_{222})v_G^{-2} - \ln Z \end{aligned} \right\}. \tag{6}$$

An isothermal-isobaric flash calculation (specified T, p and z_i) is solved iteratively. Initial; approximations for the coexisting phase compositions are estimated, equations (3) to (6) are used to find the fugacity coefficients in the gas phase and the equations (2) are used to find the K factors. In the present case, x_2 and y_1 are always small and initial estimates of the fugacity coefficients can be obtained using infinitesimal initial values for these two mole fractions. The mass balance equations may then be solved analytically to give the vapor fraction in terms of the K factors:

$$\beta = \frac{(1 - K_2) + z_1(K_2 - K_1)}{(K_1 - 1)(K_2 - 1)}. \tag{7}$$

Improved phase compositions are then obtained from the overall system composition as follows:

$$\left. \begin{aligned} x_i &= z_i / \{1 + \beta(K_i - 1)\} \\ y_i &= K_i x_i \end{aligned} \right\}, \tag{8}$$

and the calculation is repeated to convergence.

In the solubility experiment, the total amount of each component is specified along with the cell volume and temperature; consequently, an isochoric flash is required. This calculation can be done be embedding the isothermal-isobaric flash routine in an iteration loop within which the pressure adjusted until the volume occupied by the two-phase mixture matches the cell volume. This criterion can be expressed in the condition

$$p = \beta n R T Z / (V_{cell} - V_L), \tag{9}$$

where V_{cell} is the cell volume (evaluated at T and p) and V_L is the volume occupied by the liquid phase:

$$V_L = n_L (x_1 v_1 + x_2 v_2). \tag{10}$$

For practical purposes, it is useful to express the volume of the cell as a linear function of pressure as follows:

$$V_{cell} = V_0 (1 + \chi p). \tag{11}$$

In the context of the present measurements, the second and third virial coefficients of the (H_2 + H_2O) system can be obtained from independent sources (see Appendix A). So too can the molar volume of H_2O [2] and the partial molar volume of H_2 in aqueous solution [3]. The only thermodynamic parameter in the model to be fitted to the experimental is then the Henry's constant K_H; additionally, the cell-volume parameters V_0 and χ are fitted.

2.4 Experimental results

Experiments have been performed at $T = 323.15$ K with various initial gas filling pressures. The raw data obtained are typified by those plotted in Figure 2.2 and, when fitted by the model detailed in section 2.3, the parameters obtained are $k_H = 7480$ MPa, $V_0 = 88.11$ cm^3 and $\chi = 9 \times 10^{-5}$ MPa^{-1}. Figures 2.5 and 2.6 illustrate the close agreement obtained between the model and experimental data.
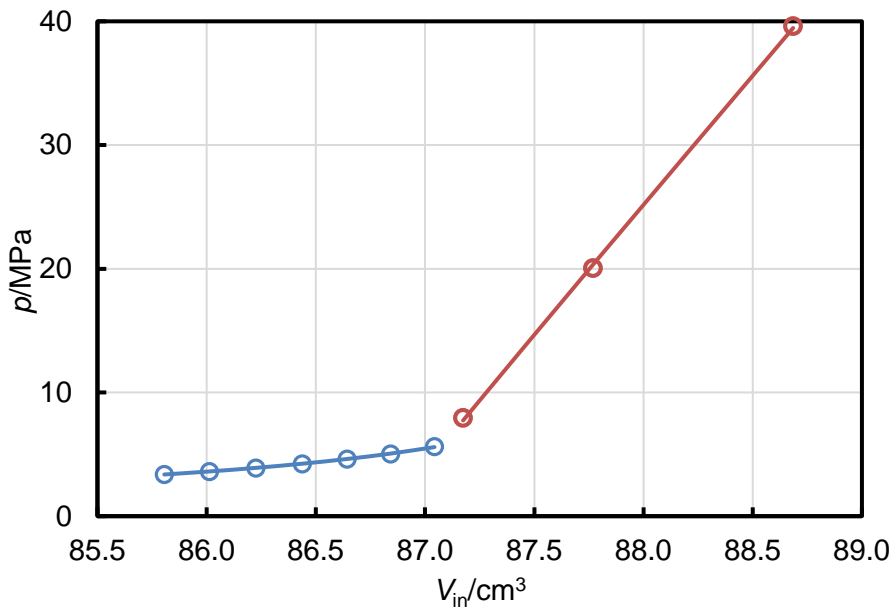

Figure 2.5: Pressures in the two-phase and single-phase regions for H_2 solubility in water at $T = 323.15$ K. Symbols:○, experiment (two phases); ○, experiment (one phase). Solid lines: thermodynamic model.
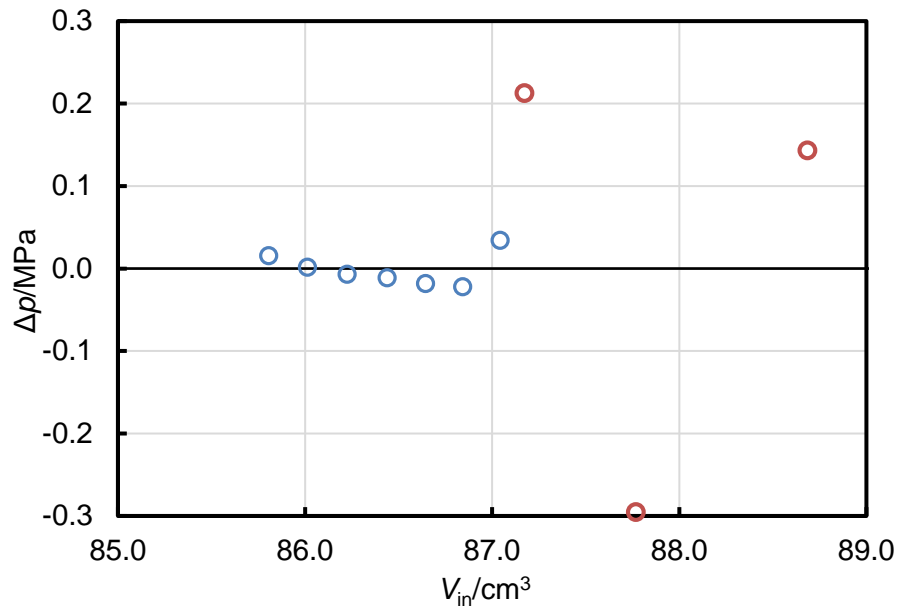
Figure 2.6: Deviations of experimental pressures in the two-phase and single-phase regions for H₂ solubility in water at T = 323.15 K. Symbols:○, experiment (two phases); ○, experiment (one phase).

The transition from two-phase to single-phase behavior was always confirmed visually. Bubble points determined from application of the thermodynamic model are found to be agree with those obtained by graphical analysis (as in Figure 2.2) are found to agree closely, usually to within 1% in pressure.

3 THERMODYNAMIC MODEL FOR THE SOLUBILITY OF HYDROGEN IN PURE WATER

In this section, we combine the new data and data from the literature and obtain the parameters of a correlative thermodynamic model that best fits the data.

3.1 Available experimental data

Experimental data for the phase behavior of ($H_2O + H_2$) have been reported by several authors and the distribution of these data by temperature and pressure is shown in Figure 3.1. Wiebe et al. [4; 5] studied the solubility of H_2 in H_2O by means of a degassing technique whereby H_2 saturated H_2O samples were expanded to low pressure and the amount of gas evolved measured in a gas burette. Their measurements are the most extensive, covering the temperature range from 273.15 K to 373.15 K with pressures up to 101 MPa. Although old, these data appear to be of very good quality. Kling and Maurer [6] studied the ($H_2O + H_2$) system temperatures between 323.15 K and 423.15 K using a synthetic variable-volume bubble-point method at pressures between 3 MPa and 15 MPa. Their results are in excellent agreement with those of Wiebe and Gaddy [4]. Pray et al. [7] report data at total pressures up to about 13 MPa at temperatures between 325 K and 616 K; unfortunately, their data at 325 K are in poor agreement with other sources. Additional data were reported by Alvarez et al. [8], Choudhary et al. [9] and Ipatiev et al. [10].
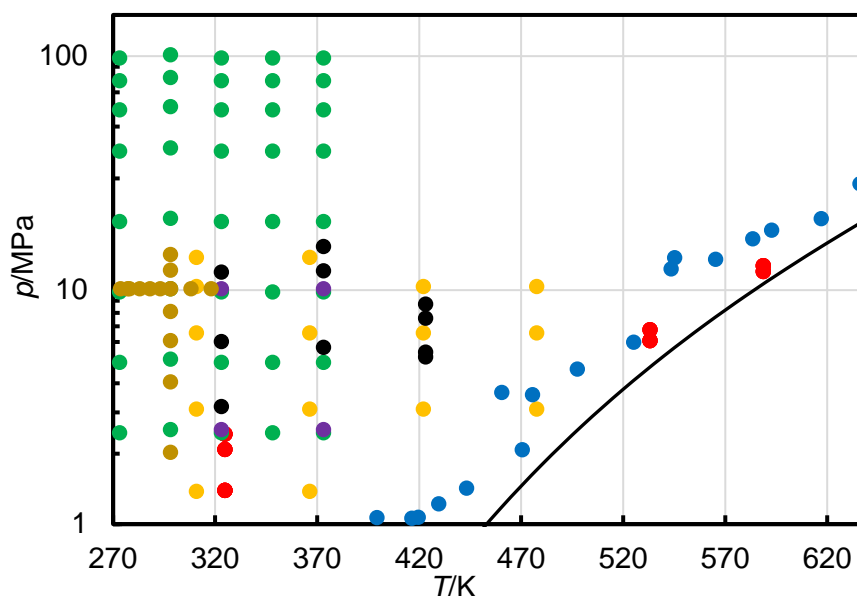

Figure 3.1: Distribution of available data in temperature-pressure space for the solubility of H_2 in H_2O. Symbols: ●, Pray et al.[7]; ●, Gillespie and Wilson [11]; ●, Wiebe et al. [4; 5]; ●, Alvarez et al. [8]; ●, Choudhary at al. [9]; ●, Ipatiev et al. [10]; ●,Kling and Maurer [6]; solid line is the vapor-pressure curve of water [12].

3.2 Thermodynamic model

The thermodynamic model detailed in section 2 of this report has been optimized to represent selected experimental data. At the present stage of the project, only data up to a maximum temperature of 373.15 K have been considered and the parameters have been fitted to the new experimental data and the literature results of Wiebe et al. [4; 5] and Kling and Maurer [6]. The second and third virial coefficients are constrained entirely by the literature and the only

parameters fitted are the Henry's constant and the partial molar volume of H_2 in aqueous solution, the latter assumed to be independent of pressure. Figure 3.2 shows the excellent agreement obtained between the data and the model. The parameters determine are shown as functions of temperature in Figure 3.3 and can be seen to be extremely smooth. This modelling approach will be extended in future work.
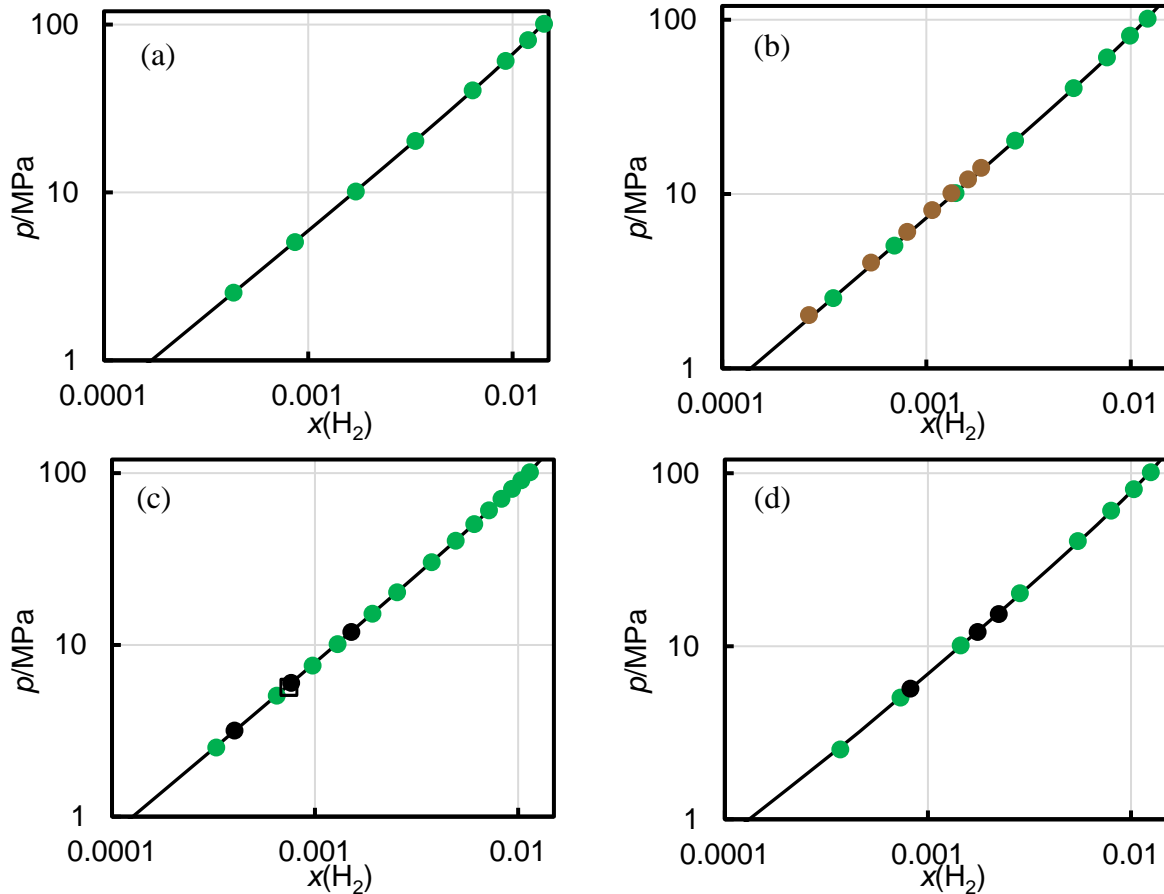

Figure 3.2: Pressure-composition diagrams for (H_2O + H_2) at (a) T = 273.15 K, (b) T = 298.15 K, (c) T =323.15 K and (d) T = 373.15 K. Symbols: ●, Wiebe et al. [4; 5]; ●, Ipatiev et al. [10] (for comparison only); ●, Kling and Maurer [6]; □, this work.

Also shown in Figure 3.3 is the correlation of Henry's constant reported by Fernández-Prini et al. based on an analysis of low-pressure data. The agreement with the current determination is reasonable but not exact. The partial molar volume obtained in the present work at T = 298.15 K is smaller than the value of (23.1 ± 1.1) cm^3/mol reported in the literature by Zhou at al. [3]. This might be in part due to the present assumption of neglecting a dependence of v_2 on pressure; it may also relate to other approximations in the model. Nevertheless, the solubility model itself provides a good account of the data and can be considered reliable in the temperature range considered here.
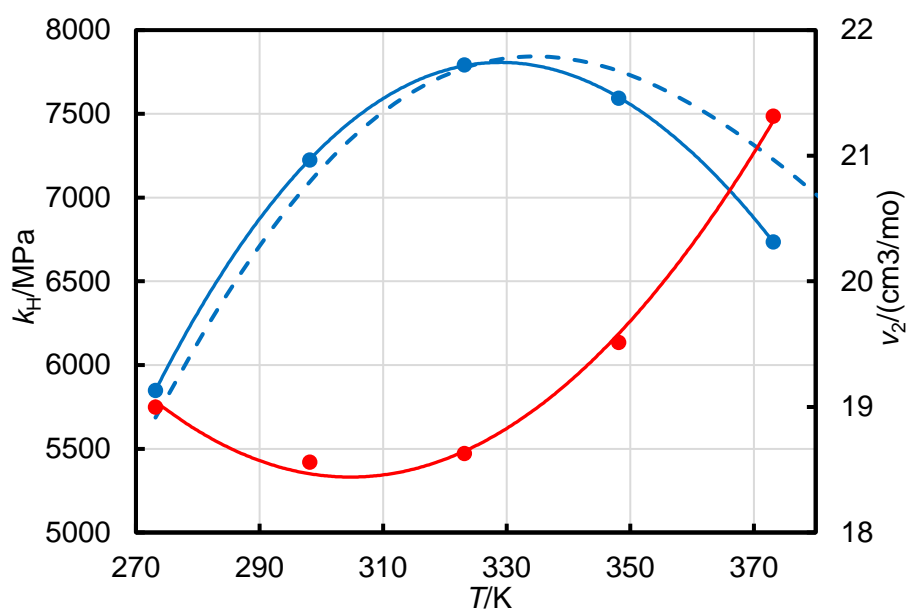
Figure 3.3: Henry's constant k_H and the partial molar volume v_2 of H_2 in aqueous solution as functions of temperature. Symbols: ●, Henry's constant; ●, partial molar volume of H_2; dashed line, Henry's constant correlation of Fernández-Prini et al. [13]; solid lines are polynomial fits to the current data.

4 CONCLUSIONS

The experimental approach to be used for the solubility of H_2 in brines has been validated in measurements of H_2 solubility in pure water. The data obtained together with extensive data from the literature have been fitted to obtain a model applicable at temperatures from 273.15 K to 373.15 K with pressures up to 101 MPa. This model will be extended to a wide temperature range in future work.

5 APPENDICES

A APPENDIX A: VIRIAL COEFFICIENTS OF THE H_2 + H_2O SYSTEM

The second and third virial coefficients of pure H_2 have been well studied by both experimental and computational means. In this work, we take the second virial coefficient B_{22} of H_2 and also the H_2-H_2O interaction second virial coefficient from the computational study of Hodges et al. [14]. These authors present a simple correlation in the form

$$B_{ij}(T) = \sum_{i=1}^{4} c_i (T^*)^{d_i}$$

(A1)

where $T^* = T/(100 \text{ K})$. The coefficients and exponents for B_{22} and B_{12} are given in Table A.1.

Table A.1: Coefficients in Equation (A1)

i	c_i	d_i	c_i	d_i
	B_{22}/(cm^3/mol)		B_{12}/(cm^3/mol)	
1	42.0803	-0.33	33.047	-0.21
2	-143.982	-1.4	-250.41	-1.5
3	146.918	-1.8	285.42	-2.26
4	-47.5601	-2.2	-186.78	-3.21

The second virial coefficient of water is well-known at high temperatures but uncertain at temperatures below about 400 K. We use the correlation recommended by Frenkel and Marsh [15], which is:

$$B_{11}(T)/(\text{cm}^3/\text{mol}) = 158.83 - 3.01 \times 10^5 (\text{K}/T) + 1.82 \times 10^8 (\text{K}/T)^2 - 5.69 \times 10^{10} (\text{K}/T)^3 . \quad \text{(A2)}$$

The third virial coefficient of pure H_2 was taken from the correlation reported by Fandiño et al. [16], which is based on the Peng-Robinson equation of state and may be written

$$C_{222}(T) = b^2 + \frac{2ab}{RT} ,$$

(A3)

where

$$a(T) = 0.457235 \left(R^2 T_c^2 / p_c \right) \left[1 + \left(0.37464 + 1.54226\,\omega - 0.26992\,\omega^2 \right) \left(1 - \sqrt{T/T_c} \right) \right]^2 ,\text{(A4)}$$

and

$$b = 0.077796\, RT_c / p_c .$$

(A5)

The parameters T_c, p_c and ω are formally the critical temperature, critical pressure and acentric factor of H_2. However, because of quantum effects at low temperature (which are absent at the temperatures of interest here) effective values are used as follows: $T_c = 31.76$ K, $p_c = 1.276$ MPa and $\omega = -0.0626$. With these parameters, equation (A3) was shown to give a good account of the available experimental data [16].

The remaining third virial coefficients, C_{111}, C_{112} and C_{122} are unknown. However, given the very small mole fraction of H_2O in the vapor phase and the mole-fraction weighting in equations (5) and (6), these terms are unimportant and were set to zero.

6   REFERENCES

[1]   J.P.M. Trusler, Annual Review of Chemical and Biomolecular Engineering 8 (2017) 381-402.

[2]   E.W. Lemmon, I.H. Bell, M.L. Huber, M.O. McLinden, NIST Standard Reference Database 23: Reference Fluid Thermodynamic and Transport Properties-REFPROP, Version 10.0, National Institute of Standards and Technology, Gaitherburg, 2018.

[3]   T. Zhou, R. Battino, J. Chem. Eng. Data 46 (2001) 331-332.

[4]   R. Wiebe, V.L. Gaddy, JACS 56 (1934) 76-79.

[5]   R. Wiebe, V.L. Gaddy, J. Conrad Heins, Ind. Eng. Chem. 24 (1932) 823-825.

[6]   G. Kling, G. Maurer, J. Chem. Thermodyn. 23 (1991) 531-541.

[7]   H.A. Pray, C.E. Schweickert, B.H. Minnich, Ind. Eng. Chem. 44 (1952) 1146-1151.

[8]   J. Alvarez, R. Crovetto, R. Fernández-Prini, 92 (1988) 935-940.

[9]   V.R. Choudhary, M.G. Parande, P.H. Brahme, Industrial & Engineering Chemistry Fundamentals 21 (1982) 472-474.

[10]   W.W. Ipatiev, S.I. Drushina-Artemovich, W.I. Tichomirov, Berichte der Deutschen Chemischen Gesellschaft 65 (1932) 568-571.

[11]   P.C. Gillespie, G.M. Wilson, Vapor-Liquid Equilibrium Data on Water-Substitute Gas Components: N_2 - H_2O, H_2 - H_2O, CO - H_2O, H_2 - CO - H_2O, and H_2S - H_2O, GPA Research Report, 1980, pp. 1-34.

[12]   E.W. Lemmon, M.L. Huber, M.O. McLinden, NIST standard reference database 23: Reference fluid thermodynamic and transport properties - REFPROP, Version 9.1, National Institute of Standards and Technology Gaithersburg, 2013.

[13]   R. Fernández-Prini, J.L. Alvarez, A.H. Harvey, J. Phys. Chem. Ref. Data 32 (2003) 903.

[14]   M.P. Hodges, R.J. Wheatley, G.K. Schenter, A.H. Harvey, J. Chem. Phys. 120 (2004) 710-720.

[15]   M. Frenkel, K.N. Marsh, Virial Coefficients of Pure Gases, Springer-Verlag Berlin Heidelberg, 2002.

[16]   O. Fandino, J.P.M. Trusler, D. Vega-Maza, Int.J. Greenhouse Gas Control 36 (2015) 78-92.